Article

A Full-Scale Test on Enhancing the Thermal Performance of a Concrete Slab Embedded with a MWCNT Heating Module Exposed to an Outdoor Environment

Sohyeon Park [1], Hoonhee Hwang [2], Heeyoung Lee [3],* and Wonseok Chung [1],*

[1] Department of Civil Engineering, KyungHee University, 1732 Deogyeong-daero, Giheung-gu, Yongin-si 17104, Republic of Korea; sohynpark@khu.ac.kr
[2] R&D Center, Korea Road Association, 26 Wiryeseoil-ro, Sujeong-gu, Seongnam-si 13467, Republic of Korea; poonhee@kroad.or.kr
[3] Department of Civil Engineering, Chosun University, 309 Pilmun-Daero, Dong-Gu, Gwangju-si 61467, Republic of Korea
* Correspondence: heeyoung0908@chosun.ac.kr (H.L.); wschung@khu.ac.kr (W.C.); Tel.: +82-62-230-7081 (H.L.); +82-31-201-2550 (W.C.); Fax: +82-62-608-5216 (H.L.)

Abstract: The aberrant winter temperatures resulting from climatic shifts give rise to the formation of imperceptible black ice on road surfaces, posing a risk of accidents. In this study, a carbon nanotube (CNT)-based heating module was fabricated, embedded in a concrete slab, and subjected to a full-scale test in an outdoor environment. Preliminary tests were conducted to scrutinize the thermal behavior of the CNT heating modules applied to the concrete slab, considering the inter-module distance and the concentration of multiwalled carbon nanotubes (MWCNTs) in the concrete perimeter. A full-scale concrete slab was fabricated on the basis of the preliminary test results. Thermal performance analyses of the concrete perimeter were performed according to the MWCNT concentration, the distance between the MWCNT heating modules, and the supply voltage based on a full-scale test conducted in an outdoor environment. The full-scale test results indicated that the maximum temperature variation of the MWCNT heating module embedded concrete slab was 46.8 °C, and its thermal performance varied by 1.9 times depending on the concentration of MWCNTs in the concrete perimeter.

Keywords: black ice; CNT heating module; concrete slab; thermal performance; outdoor environment

1. Introduction

Black ice, an imperceptible and thin ice layer on road surfaces, poses a hazard leading to accidents during winter periods. Historically, preventive measures against freezing involved the application of deicing chemicals sprayed onto the road [1]. These chemicals increase the maintenance cost by causing rapid deterioration and damage to road surfaces and structures [2]. Deicing chemicals also corrode the substructures of the road and destroy soil ecosystems [3,4]. To resolve these problems with deicing chemicals, methods were developed to embed heating wires in pavements [5–7]. When voltage is applied to the pavement with embedded steel heating wires, the heat generated from the wires removes the black ice deposited on the upper surface of the pavement. However, when steel heating wires are continuously used, corrosion occurs and resistance increases, thereby causing an increase in electric power requirements [8,9]. Hence, in recent years, studies have been conducted to generate heat from concrete structures by adding carbon-based nanomaterials.

Carbon-based nanomaterials have been used in many studies as heating materials in concrete structures owing to their high thermal and electrical conductivity [9–13]. Through initial studies that mixed carbon-based nanomaterials with concrete, we gathered the thermal efficiency under several conditions. The conditions included the type of carbon-based nanomaterials, the concentrations, the voltages, the heating time, etc. Almost all the initial study's tests were conducted in laboratories by preparing cubic-type specimens. A

cubic-type specimen is defined as a cube or cuboid specimen of a size that can be tested in the laboratory. In other relevant studies, cubic-type heating cementitious composites (size = $25 \times 25 \times 25$ mm^3) mixed with carbon nanotubes (CNTs) were fabricated in laboratories, and their thermal performance was analyzed according to the nanomaterials' concentration and voltage. The concentration of CNTs was set in the range of 0.1–2 wt%, and the voltage was applied in stages in the range of 3–20 V. In the test results, the thermal performance of heating cementitious composites was improved as the concentration of CNTs increased; accordingly, the highest thermal efficiency was observed when the concentration of CNTs was ≤0.6 wt% [14]. In a thermal performance analysis study conducted according to the type of carbon-based nanomaterial, cubic-type specimens were prepared using carbon-based nanomaterials, including multiwalled carbon nanotubes (MWCNTs), graphene nanoplatelets (GNPs), and carbon black (CB). The temperature variation increased as the concentration of nanomaterials increased owing to the formation of multiple networks inside the composite; a maximum temperature variation of 67.5 °C occurred when MWCNTs were added [15]. Another study focused on the electrical performance of the heating cementitious composites that incorporated MWCNTs. The analyzed results showed that the electrical resistance of the heating cementitious composites decreased as the concentration of MWCNTs increased [11]. CNTs and silica aerogels were added into cubic-type specimens, and the thermal performance of the cementitious composites was analyzed [16]. The specimens were prepared by adding silica aerogels to polymer composites (at concentrations of 0, 0.5, and 1%) that contained 4% CNTs. The electrical properties of these specimens were analyzed based on the quantification of their tunneling and thermal performance under circulation and long-term heating conditions. The test results showed that the addition of silica aerogels increased the cooling time and improved the thermal performance of the composites by reducing the CNT particles. In the same manner, thermal performance tests were conducted with cubic-type specimens by applying various mixing methods, including MWCNT solutions, films, and a combination of solution and films. The concentration of MWCNTs was set to 0.0, 0.125, 0.25, and 0.5 wt%, while the supply voltage was set to 10, 20, 30, and 60 V. Consequently, the specimen with both the MWCNT solution and films yielded the highest temperature of 77.5 °C [17].

In subsequent laboratory studies related to heating cementitious composites, specimens were prepared in various sizes (instead of using simple cubic-type specimens) to analyze the effects of size [18–26]. To explain some of the studies, the thermal performance of heating cementitious composites mixed with CNTs were analyzed using specimens with a length of 100 mm, a width of 20 mm, and a height of 20 mm. Two voltage settings (50 and 100 V) were applied in two cycles (supply for 6 h and resting for 2 h). The thermal performance of the heating cementitious composites improved as the concentration of CNTs increased, and the largest temperature variation was observed when the concentration of CNTs was 0.5 wt%. However, when a long-term heating test was conducted, the thermal performance of the heating cementitious composites decreased [18]. In another study, bar specimens (size = $25 \times 26 \times 150$ mm^3) were prepared by adding silica fume to heating cementitious composites; four copper plates were installed at 18 mm intervals as electrodes. Twelve mixtures were prepared and tested by adjusting the ratio between the CNTs and the silica fume. It was found that mechanical breakage occurred when a small amount of silica fume was mixed with CNT particles. As the content of silica fume increased, the CNTs' dispersibility improved, but the dispersed CNTs agglomerated again and formed lumps. Consequently, the electrical resistance of the composites decreased [19]. In another study, heating cementitious composites (size = $40 \times 40 \times 160$ mm^3) were fabricated and artificial defects were formed to analyze the thermal performance and its variations owing to these defects. The thermal performance of the heating cementitious composite was reduced by up to 40% when the cross-sectional area was reduced by 50% owing to the artificial defects [20]. CNTs were added into specimens (size = $40 \times 40 \times 160$ mm^3), and heating cementitious composites were fabricated. The thermal performance of CNTs was then analyzed according to the defects' size. The analyzed results showed that the temperature

variation of the heating cementitious composites was reduced by up to 48% when the defects' size increased to 75% of the total cross-sectional area [21].

In most other studies [8–21], the thermal performance of heating cementitious composites was analyzed in laboratories indoors. Hence, studies have been recently conducted to analyze the thermal performance of heating cementitious composites in outdoor environments [8,22,27–44]. In these studies, a concrete slab (size = 3000 × 3000 × 100 mm^3) was fabricated in an outdoor environment, and CNT heating modules were embedded in the center of the concrete slab. When the heating test was conducted for 12 h, snowmelt was visually evident on the concrete slab, and a temperature higher than the outdoor air temperature (by 6.4 °C) was measured [22]. In a study on snowmelt on outdoor airport pavements, a melting test was conducted based on the use of carbon fiber, and grille-reinforced composites. In the test, the rate of snowmelt in the entire area was analyzed; all the snow on the top surface of the concrete slab melted when heat was generated for 3.5 h [27]. Additionally, studies have been conducted experimenting with the thermal properties of cementitious composites using nanomaterials other than CNT [8,28–44].

In previous studies related to the heating of cementitious composites in outdoor environments [8,22,27–44], tests were conducted to generate heat in concrete slabs, and the presence of snowmelt attributed to the generated heat was confirmed. However, the optimized heating modules for use in a concrete slab were not examined. Therefore, this study undertook a laboratory test to examine the thermal performance of carbon nanotube (CNT) heating modules. The investigation focused on variations in the concentration of multiwalled carbon nanotubes (MWCNTs) along the concrete perimeter and the spacing between the MWCNT heating modules, aiming to optimize their embedding pattern within the concrete slab. Based on the optimized MWCNT heating modules, a MWCNT heating module embedded concrete slab was fabricated as shown in Figure 1 to conduct a full-scale test in an outdoor environment. In the full-scale test, an attempt was made to analyze the thermal performance according to the concentration of MWCNTs in the concrete perimeter, the distance between MWCNT heating modules, and the supply voltage. The temperature variation as a function of the distance between the MWCNT heating modules was analyzed at each supply voltage setting to identify correlations between the factors.
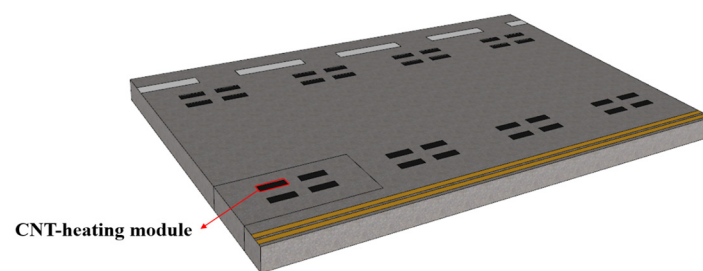
Figure 1. Concept of MWCNT heating modules embedded in a concrete slab.

Therefore, this study aimed to present a model with low construction cost, durability, and secure constructability from a long-term perspective to solve the problem of black ice. The new model proposed in this study was a concrete slab embedded with a MWCNT heating module. The MWCNT heating module incorporated nanomaterials into the concrete slab, and the module (the MWCNT heating module) with heating performance was inserted in a continuous manner at the place where the vehicle wheels pass on the road surface slab to melt black ice. Several parameters were set and experimented with so that the MWCNT heating module could show optimal heating performance in the slab. The parameters were set as the concentration of nanomaterials (MWCNTs) incorporated in the MWCNT heating module itself, the MWCNT heating modules' spacing, the incorporation of the concrete around the MWCNT heating module, and the supply voltage.

2. Laboratory Test

2.1. Test Outline

In the laboratory test, the thermal performance of MWCNT heating modules was analyzed. The MWCNTs are a product of Company D, with an average diameter of 95 nm and an average length of 1.5 μm. For the laboratory test specimens, two cubic MWCNT heating modules (size = $50 \times 50 \times 50$ mm^3) were embedded in a rectangular parallel-piped concrete slab (size = $400 \times 100 \times 50$ mm^3). The concentration of MWCNTs in the concrete perimeter and the distance between the MWCNT heating modules were set as the parameters (Table 1).

Table 1. Laboratory test parameters.

Concentration of Multiwalled Carbon Nanotubes (MWCNT) in the Concrete Perimeter (wt%)	Distance between Carbon Nanotube (CNT) Jheating Modules (mm)	Specimen Name
0.0	100	C0.0-D100
	150	C0.0-D150
	200	C0.0-D200
	250	C0.0-D250
	300	C0.0-D300
	350	C0.0-D350
0.2	100	C0.2-D100
	150	C0.2-D150
	200	C0.2-D200
	250	C0.2-D250
	300	C0.2-D300
	350	C0.2-D350
0.5	100	C0.5-D100
	150	C0.5-D150
	200	C0.5-D200
	250	C0.5-D250
	300	C0.5-D300
	350	C0.5-D350
1.0	100	C1.0-D100
	150	C1.0-D150
	200	C1.0-D200
	250	C1.0-D250
	300	C1.0-D300
	350	C1.0-D350

The size of the laboratory test specimen was set by referring to a previous study in which the thermal performance was analyzed by setting the size of the heating cementitious composites mixed with carbon-based nanomaterials to $50 \times 50 \times 50$mm^3 [15–17,45–47]. In a previous study, thermal performance above a certain level was achieved when the distance between heating points ranged from 80 to 160 mm. Therefore, in this study, the concentration of MWCNTs in the MWCNT heating module was fixed at 1.0 wt% with reference to a previous study [48], and the concentration of MWCNTs in the concrete perimeter was set to 0.0, 0.2, 0.5, and 1.0 wt% compared with the weight of the cement.

The distance between the centers of the CNT heating modules was set to 50, 100, 150, 200, 250, and 300 mm so that the spacing between the two modules could be adjusted after embedding. The MWCNT heating modules were embedded after curing for 1 day because their shapes can be deformed during preparation of the specimens. The completed specimens were cured for 7 days. A voltage of 60 V was supplied to the MWCNT heating module for 60 min [16].

The specimen names in the laboratory test were expressed by using the concentration of MWCNT in the concrete perimeter and the distance between the MWCNT heating modules. The first part of each coded name, "C", represents the concentration of MWCNTs in the concrete perimeter, which is the first letter of the term "concentration", and is reported together with the concentration of nanomaterial. Thus, "C1.0" indicates that the concentration of nanomaterials is 1.0 wt% compared with the weight of the cement. The second part represents the distance between the MWCNT heating modules, indicated by "D," which is the first letter of distance; this is reported together with the distance between the modules. Thus, "D150" indicates that the distance between the CNT heating modules is 150 mm.

The cement used for the fabrication of the MWCNT heating modules and the concrete slab for the full-scale test was Type 1 ordinary Portland cement. For sand, KS L ISO 679 standard [49] sand was used. For MWCNTs, a functionalized aqueous solution with a purity of ≥99.9% was used to ensure the dispersibility. The MWCNT solution was dispersed in polyacrylic acid for 2 h using ultrasound at 22 kHz [11,17,48,50]. A stainless-steel material was used for the electrodes to apply voltage to the heating cementitious composite. The temperature of the central part of the MWCNT heating module was measured using a thermocouple.

Figure 2 shows the fabrication process of the MWCNT heating modules. First, the solution of nanomaterials, cement, and standard sand were measured according to the mix design (Figure 2a). The water-to-cement ratio used for the fabrication of the MWCNT heating module was 50%, and the weight ratio of the aqueous solution, cement, and standard sand was 1:2:5 (40 g:80 g:200 g). The cement and sand were dry-mixed for 2 min to ensure the material's homogeneity, as shown in Figure 2b. Figure 2c shows the process of adding and mixing the MWCNT solution during a 3-min period. The cementitious composite was poured into the mold in three layers after mixing, and compaction was performed 30 times for each layer (Figure 2d). Two stainless-steel meshes were then inserted at 20 mm intervals (Figure 2e).

Finally, a thermocouple was inserted into the center of the heating cementitious composite at a depth of 25 mm to measure the internal temperature during the heating test. The MWCNT heating module was cured for 24 h to maintain the shape; it was then inserted during preparation of the specimen. Two MWCNT heating modules were used per specimen. Figure 2g shows the process of compaction after the adjustment of the distance between the MWCNT heating modules and the concentration of MWCNTs in the concrete perimeter in the specimen's mold. Finally, a thermocouple was installed at the middle point between the MWCNT heating modules at a depth of 25 mm to measure the internal temperature during the heating test (Figure 2h). The completed specimen for the laboratory test was subjected to dry-air curing for 7 days.

Figure 3 shows the laboratory test setup. The test was conducted by applying a constant voltage of 60 V for 60 min. The voltage was applied to the installed specimen via a direct current (DC) power supply (EX-200, ODA Technology, Incheon, Korea). The temperature variation was measured every 2 s by connecting the thermocouples installed in the MWCNT heating modules to a data logger (TDS-303, Tokyo Sokki Kenkyujo Co., Ltd., Tokyo, Japan).
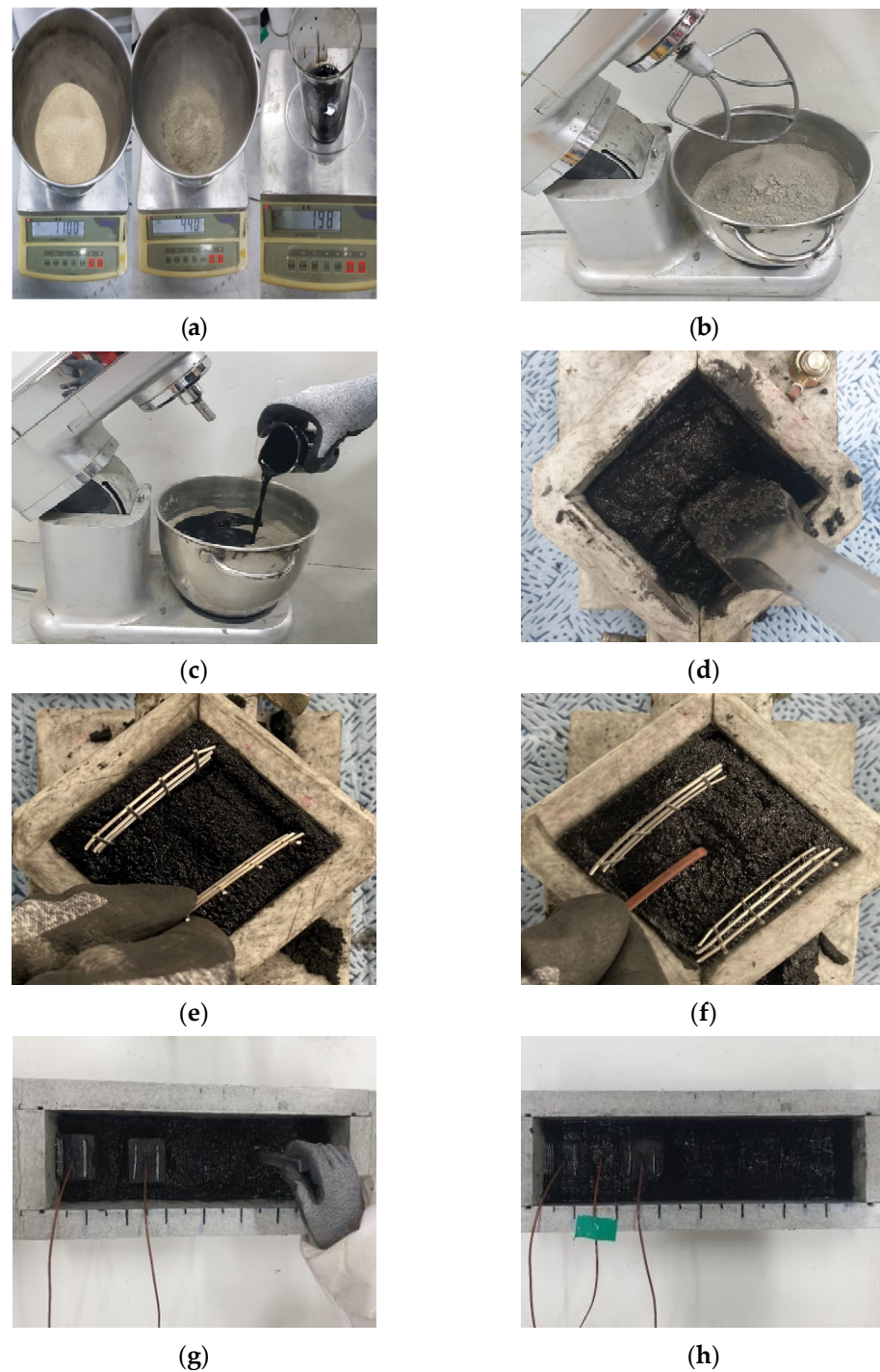
Figure 2. Fabrication process of the specimens used in laboratory tests. (**a**) Measurement of the materials. (**b**) Dry mixing (2 min). (**c**) Mixing the MWCNT solution (3 min). (**d**) Compaction. (**e**) Insertion of the stainless-steel mesh. (**f**) Insertion of the thermocouple. (**g**) Compaction. (**h**) Insertion of the thermocouple.
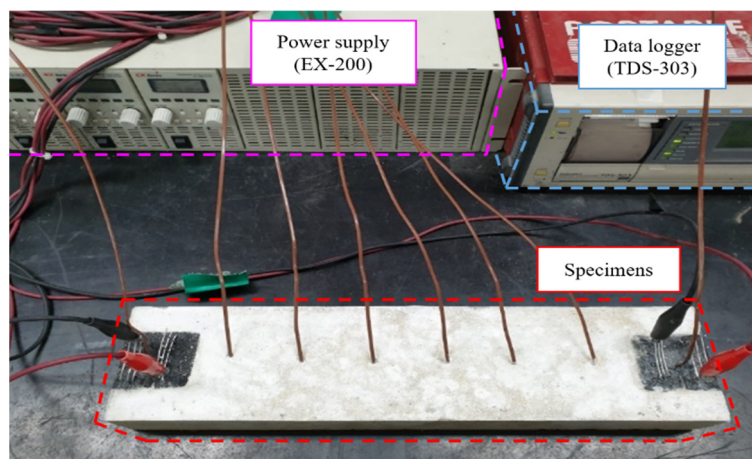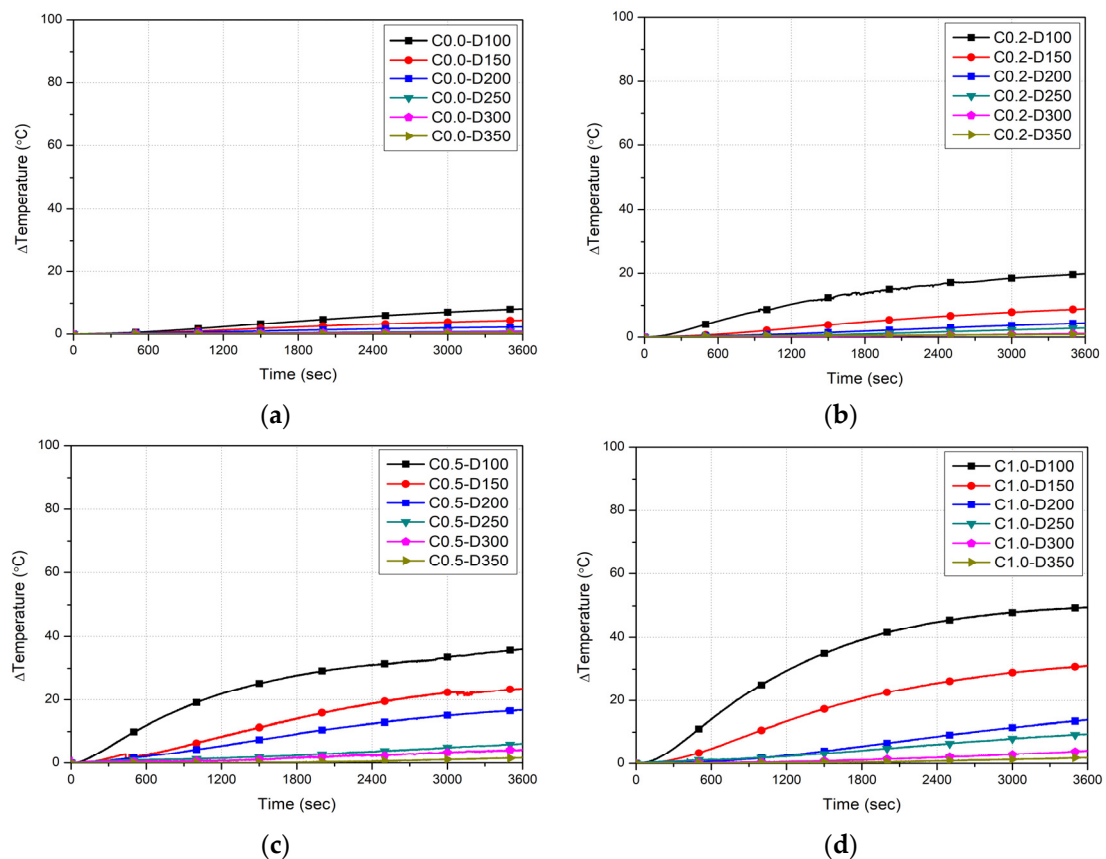
Figure 3. Laboratory test setup.

2.2. Laboratory Test Results

Figure 4 shows the temperature variation of the concrete perimeter according to the distance between the MWCNT heating modules at all concentrations of MWCNTs in the laboratory test specimens. The maximum temperature variations of the parameters associated with the laboratory test are listed in Table 2. The test results showed that the temperature variation increased as the concentration of MWCNTs increased from 0 to 1.0 wt%. In Figure 4a, the control specimen for which the concentration of MWCNTs in the concrete perimeter was 0 wt% exhibited a temperature variation of 0.3 °C when the distance between the MWCNT heating modules was maximized (350 mm). As the distance decreased by 50 mm, the temperature variation of the laboratory test specimen increased. However, the maximum temperature variation was only 8.5 °C when the distance reached 100 mm. For the specimen with an MWCNT concentration of 0.2 wt%, the temperature variation increased to 0.9 °C at the maximum distance (350 mm), and it increased to 20.0 °C when the distance was 100 mm (Figure 4b). In Figure 4c, the temperature variation of C-C0.5-D350 increased over time to 4.0 °C. The temperature variation of C-C0.5-D100 increased to 39.6 °C; this outcome was twice as high as the variation obtained when the concentration of MWCNTs was 0.2 wt%. When the concentration of MWCNTs in the concrete perimeter was maximized (1.0 wt%), the maximum temperature variation was 5.1 °C in the case of the largest distance between the MWCNT heating modules (350 mm), and it increased to 50.8 °C in the case of the smallest distance between the MWCNT heating modules (100 mm) (Figure 4d).

The MWCNT heating modules installed in the laboratory test specimens showed different temperature variations even though the modules were fabricated under the same conditions. For this reason, the ratio of the temperature of the MWCNT heating module to the temperature of the center of the specimen was compared to analyze the thermal performance according to the distance between the MWCNT heating modules. Figure 5 shows the trendlines of the center/CNT heating module thermal ratios as a function of the distance between the MWCNT heating modules obtained in laboratory tests. Based on the laboratory test results, the trendline as a function of distance is shown in Figure 5a. The trendline was expressed in the form of $y = e^{-ax}$, and the reliability of the trendline was examined via the R^2 value, which was higher than 0.96. In this study, it was predicted that the temperature of the center of the specimen would become identical to that of the MWCNT heating module when the distance between the center of the specimen and the MWCNT heating module converged to 0 mm. For this reason, the thermal ratio was assumed to be 100% in this study when the interval distance was 0 mm. Subsequently, the thermal ratio decreased as the interval distance increased. Figure 5b shows the trendline of the thermal ratio in the indoor experiment according to the concentration of MWCNTs. When the concentration of MWCNTs was 0 wt%, the thermal ratio decreased abruptly as

the distance between the MWCNT heating modules increased. When the concentration of MWCNT was 0.2 wt%, the thermal ratio slightly increased by ≤0.5 times as a function of the interval distance compared with that at 0 wt%. When the concentration of MWCNTs was increased to 0.5 wt%, the thermal ratio increased by at most 3.3 times compared with that at 0 wt%. The specimen with an MWCNT concentration of 1.0 wt% yielded the largest increase in the thermal ratio (4.6 times) compared with that at 0 wt%. As the minimum design temperature of a concrete structure is considered to be equal to −17.8 °C according to the American Association of State Highway and Transportation Officials (AASHTO) LRFD bridge design specifications, the design temperature variation was set to 17.8 °C in this study to maintain the concrete at room temperature [51]. In this study, the average maximum temperature variation of the MWCNT heating modules was 66 °C. Therefore, the minimum thermal performance was expected to be realized when the central/MWCNT heating module thermal ratio was ≥20%. Therefore, the minimum thermal performance was achieved when the interval distances were ≤150 mm for MWCNT concentrations of ≤0.2 wt%, ≤270 mm for 0.5 wt%, and ≤300 mm for 1.0 wt%. Although the number of MWCNTs used was doubled for an MWCNT concentration of 1.0 wt% compared with 0.5 wt%, the maximum difference in the thermal ratio was 21%. This indicated that the most efficient concentration of MWCNTs was 0.5 wt%. Considering that the full-scale test was performed in an outdoor environment, the central/MWCNT heating module thermal ratio was ≥40%. Therefore, the maximum interval distance of the MWCNT heating modules was determined to be 150 mm.

**Figure 4.** Temperature variation at the middle point between the heating modules in the laboratory test. (**a**) C0.0. (**b**) C0.2. (**c**) C0.5. (**d**) C1.0.

Table 2. Maximum temperature variations in the laboratory tests (°C).

		Distance between CNT Heating Modules (mm)					
		100 (D100)	150 (D150)	200 (D200)	250 (D250)	300 (D300)	350 (D350)
MWCNT concentration (wt%)	0.0 (C0.0)	8.5	4.7	2.4	1.0	0.8	0.3
	0.2 (C0.2)	20.2	9.2	4.7	3.1	1.3	0.9
	0.5 (C0.5)	39.6	26.8	19.9	9.8	8.5	4.0
	1.0 (C1.0)	50.8	34.1	20.2	13.9	9.0	5.1
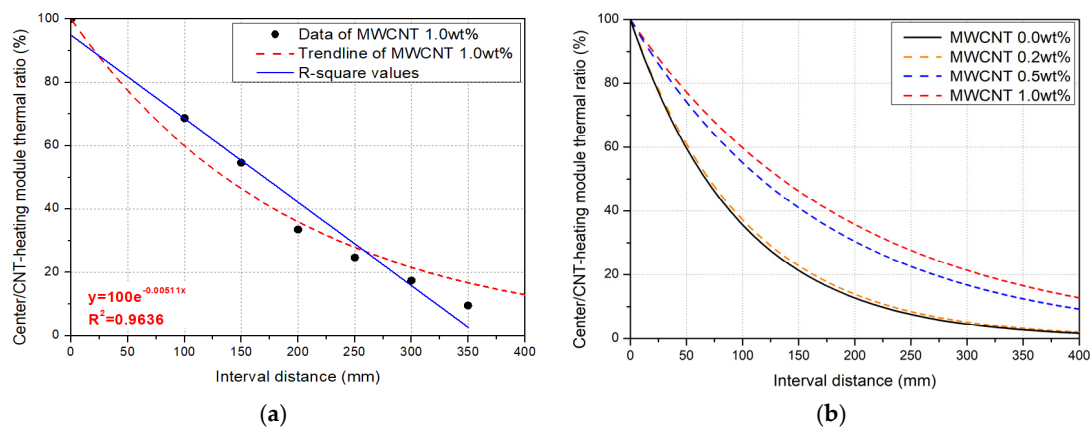
Figure 5. Trendlines of the thermal ratio as a function of the distance between MWCNT heating modules in laboratory test. (**a**) Example of the relationship between the thermal ratio and the interval distance. (**b**) Thermal ratios as a function of the interval distance at different concentrations of MWCNTs.

The surface temperature and heat distribution of the laboratory test specimens were measured via the thermal images in Figure 6. For C1.0-D100, the temperature at the middle point between the MWCNT heating modules was the highest (approximately 60 °C) as the distance between the MWCNT heating modules was the smallest (100 mm) (Figure 6a). In Figure 6b,c, the temperature at the middle point decreased to 44 °C and 35 °C as the distance increased to 150 and 200 mm, but the heat released from the MWCNT heating modules overlapped. For C1.0-D250 and C-C1.0-D300, the distance between the CNT heating modules increased and the temperature at the middle point decreased to 28 °C and 26 °C, respectively; these values were 47% and 43% of those of C1.0-D100 (Figure 6d,e). In the case of C1.0-D350, which had the largest distance between the MWCNT heating modules (Figure 6f), the temperature variation induced by the MWCNT heating modules was not observed at the middle point, and the temperature at that point was similar to the outdoor air temperature.
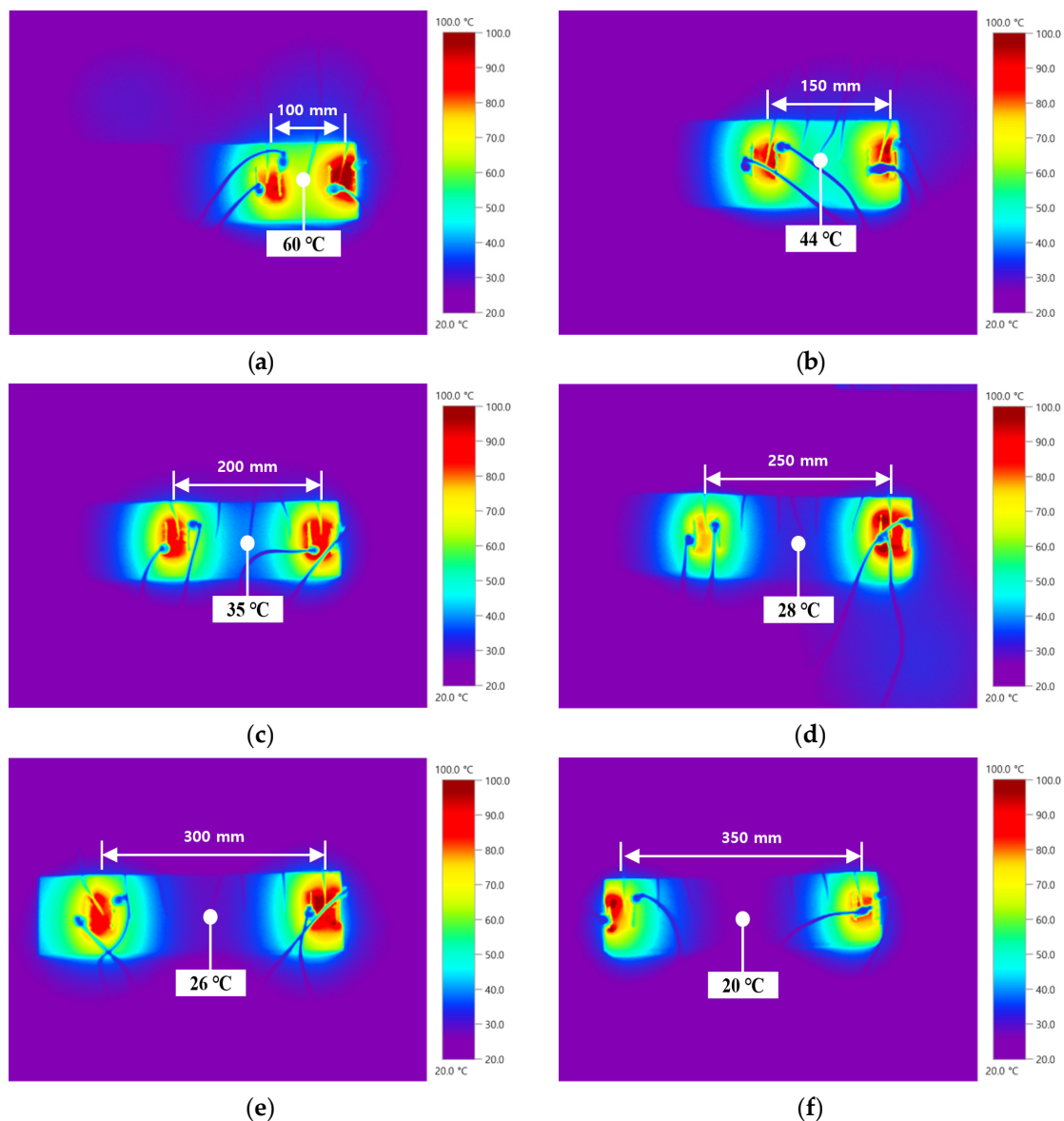
Figure 6. Thermal images of the MWCNT heating modules used in the laboratory tests. (**a**) C1.0-D100. (**b**) C1.0-D150. (**c**) C1.0-D200. (**d**) C1.0-D250. (**e**) C1.0-D300. (**f**) C1.0-D350.

3. Full-Scale Test in an Outdoor Environment

3.1. Test Outline

In the second step, a MWCNT heating module embedded in a concrete slab was fabricated first, followed by the execution of a full-scale test in an outdoor environment. The MWCNT heating module applied during the fabrication of the full-scale concrete slab was fabricated in line with the thermal performance according to the parameters derived in the previous laboratory test. The size of the embedded concrete slab with the MWCNT heating module was $6000 \times 3000 \times 250$ mm^3. To perform tests according to the parameters in one slab, sections were divided and four MWCNT heating modules (sizes = $300 \times 100 \times 60$ mm^3) were installed in an area of 1500×800 mm^2 per parameter. Therefore, in this study, the size of the MWCNT heating module applied in the full-scale test was optimized and was set to $300 \times 100 \times 50$ mm^3. The concentration of MWCNTs in the concrete perimeter, the distance between MWCNT heating modules, and the supply voltage were set as the parameters of the full-scale test. The concentration of MWCNTs in the MWCNT heating module itself was fixed at 1.0 wt% as in the previous laboratory

test, and the concentration of MWCNTs in the concrete perimeter was set to 0.0 and 0.5 wt% compared with the weight of the cement. The distance between the MWCNT heating modules was set to 50, 100, and 150 mm, while the supply voltage was set to 30 and 60 V.

The names of the test units in the full-scale test were expressed by using the concentration of MWCNTs in the concrete perimeter, the distance between the MWCNT heating modules, and the supply voltage, in sequence. The first part of each coded name represents the concentration of MWCNTs in the concrete perimeter and is denoted by the first letter of the term "concentration"; this is reported together with the concentration of nanomaterials. Thus, "C1.0" indicates that the concentration of nanomaterials was 1.0 wt% compared with the weight of cement. The second part represents the distance between the MWCNT heating modules and is denoted by the first letter of the term "distance"; this is reported together with the interval distance. Thus, "D150" indicates that the distance between the MWCNT heating modules was 150 mm. The third part represents the supply voltage and is denoted by the first letter of the term "voltage"; this is reported together with the supply voltage. Thus, "V30" means that a voltage of 30 V was applied during the heating test. Figure 7 shows the fabrication process of the full-scale test unit.


| (a) | (b) |
| (c) | (d) |
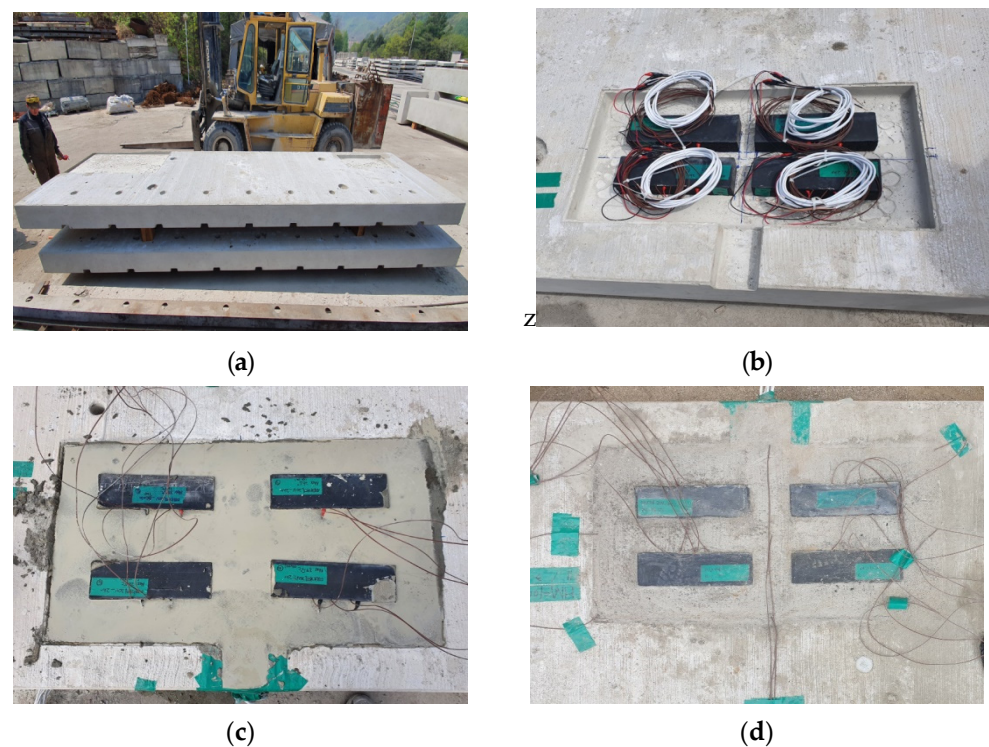
Figure 7. Fabrication process of the test unit for the full-scale test. (**a**) Fabrication of the precast concrete slab. (**b**) Arrangement of the MWCNT heating modules. (**c**) Pouring the concrete. (**d**) Insertion of the thermocouple and curing.

A precast concrete slab was fabricated to install the MWCNT heating modules (Figure 7a). The MWCNT heating modules were arranged according to the distance (50, 100, and 150 mm) in the fabricated slab (Figure 7b). In this instance, the wires installed in the MWCNT heating modules to supply voltage were arranged through the grooves; these were prepared in advance in the precast concrete slab. The concrete produced by measuring the nanomaterial solution or water, cement, and standard sand based on the mix's design was poured around the arranged MWCNT heating modules, as shown in Figure 7c. Finally, thermocouples were installed to measure the internal temperature during the heating test, followed by curing (Figure 7d).

Figure 8 shows the full-scale test setup. Two voltages (30 or 60 V) were applied for 60 min. The voltage was supplied by the same DC power supply, and the voltage was ap-

plied after the (+) and (−) electrodes were connected to the stainless-steel meshes installed in the MWCNT heating modules. The rate of increase in the internal temperature of the MWCNT heating module as a function of the supply voltage was measured by connecting the thermocouples installed during the specimen's preparation to the data logger.
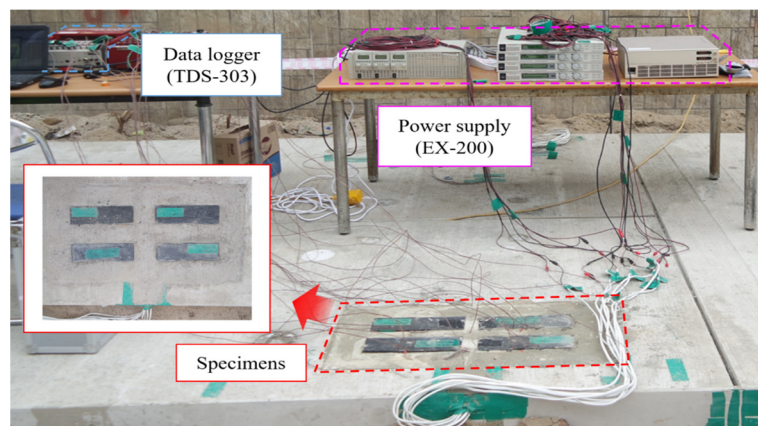

Figure 8. Full-scale test setup.

3.2. Full-Scale Test Results

Figure 9 shows a plot of the temperature variation as a function of the distance between the MWCNT heating modules in the full-scale test in an outdoor environment. The maximum temperature variations associated with the parameters are also presented (Table 3). Figure 9a shows the temperature variation of C0.0-D50 over time. The maximum temperature variation of C0.0-D50 was 13.3 °C at 30 V and 32.3 °C at 60 V. When the voltage was doubled, the temperature variation increased by 2.4 times. In Figure 9b, the maximum temperature variation of C0.0-D100 was measured to be 10.7 °C at 30 V and 23.5 °C at 60 V. The temperature variation increased by 2.2 times as a function of the voltage. For C0.0-D150, which had the largest interval distance among the test units with an MWCNT concentration of 0 wt%, the maximum temperature variation was 7.4 °C at 30 V and 15.7 °C at 60 V (Figure 9c). The temperature variation increased by 2.1 times as the voltage increased. Compared with C0.0-D50, the temperature variation decreased by up to 27% for C0.0-D100 and by up to 51% for C0.0-D150. Considering the design temperature variation (17.8 °C) based on the AASHTO LRFD bridge design specifications [51], it was predicted that the minimum temperature variation would occur if a voltage higher than 60 V was supplied when the distance between the MWCNT heating modules was 150 mm. For C0.0-D100 and C0.0-D50, which had interval distances of ≤100 mm, the temperature variation exceeded the design temperature variation when the supply voltage was set to 60 V.

Figure 10 shows the thermal performance as a function of the distance between the CNT heating modules. The trendlines were expressed in the form of $y = e^{-ax}$, and their R^2 values were found to be ≥0.98. When the concentration of MWCNTs in the concrete perimeter was 0 wt% at a supply voltage of 30 V, an interval distance of ≤25 mm was required for the temperature variation to exceed the design temperature variation (17.8 °C). At a supply voltage of 60 V, the temperature variation exceeded the design temperature variation (17.8 °C) when the distance between the MWCNT heating modules was maintained at values of ≤125 mm. For the embedded concrete slab (with the MWCNT heating module) in which the concentration of MWCNTs in the concrete perimeter was 0 wt%, the supply voltage had to be set to values of ≥60 V because it was difficult to develop the desired thermal performance when the supply voltage was set to 30 V. In addition, when a voltage of 60 V was applied to the embedded concrete slab, excellent thermal performance was observed at interval distances of ≤125 mm. In this study, it was possible to predict the thermal performance according to the distance between the MWCNT heating modules based on the tendency of the temperature variation.
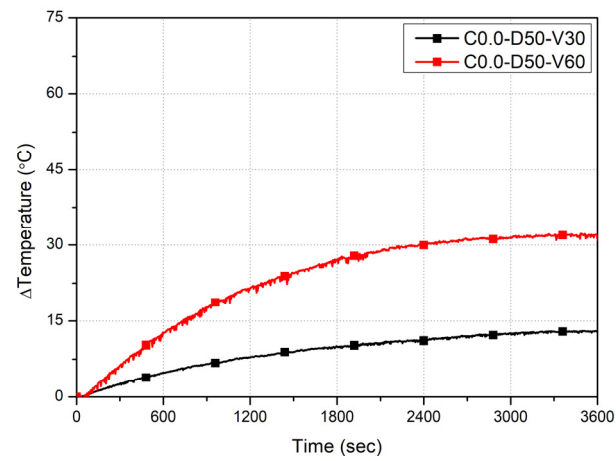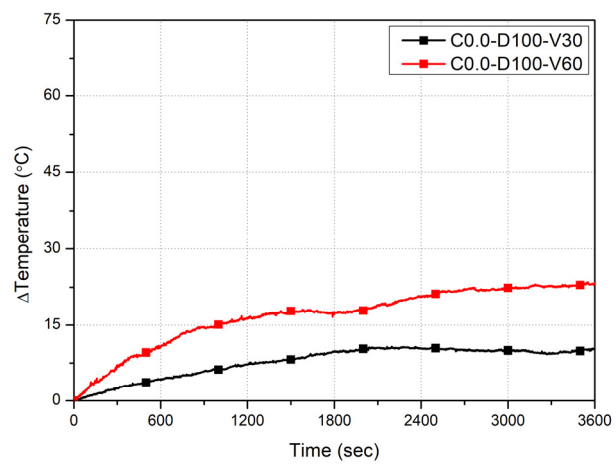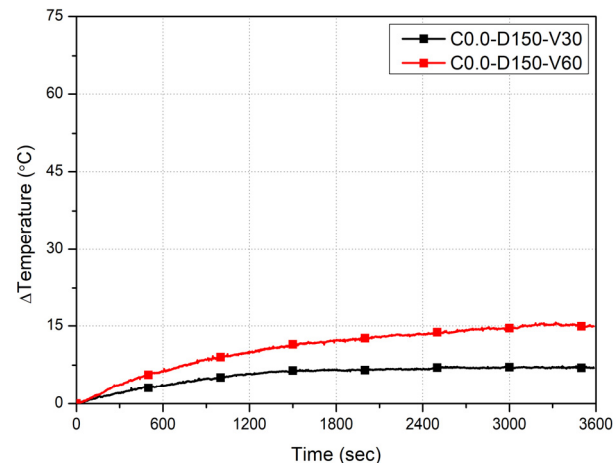
Figure 9. Temperature variation of MWCNT heating modules in the full-scale test. (**a**) C0.0-D50. (**b**) C0.0-D100. (**c**) C0.0-D150.

Table 3. Maximum temperature variations in the full-scale test (°C).

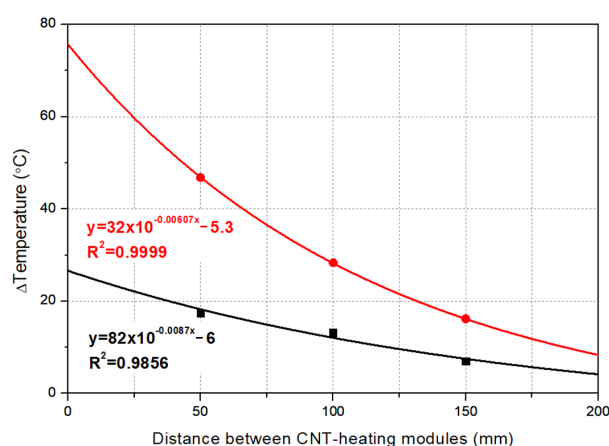| Concentration of MWCNTs (wt%)	Distance between MWCNT heating modules (mm)	Supply Voltage (V)	
		30	60
0.0 (C0.0)	50 (D50)	13.3	32.3
	50 (D100)	10.7	23.5
	150 (D150)	7.4	15.7
0.5 (C0.5)	100 (D100)	18.6	44.7

Figure 10. Thermal performance as a function of distance between MWCNT heating modules.

Figure 11 shows the temperature variation when the concentration of MWCNTs in the concrete perimeter was 0.0 and 0.5 wt% in the full-scale test conducted in an outdoor environment. The concentration of MWCNTs in the concrete perimeter was set to 0.5 wt% according to the analyzed results in the previous laboratory test. As the minimum temperature variation developed when the interval distances were ≤150 mm in the case of the specimen with an MWCNT concentration of 0.0 wt%, the distance between the MWCNT heating modules was set to values of ≤150 mm in the full-scale test conducted in an outdoor environment. As the temperature variation exceeded the design temperature variation (17.8 °C) at a supply voltage of 60 V and at an interval distance equal to 100 mm in instances in which the concentration of MWCNTs in the concrete perimeter was 0 wt%, the distance between the MWCNT heating modules was fixed at 100 mm. In Figure 11a, the maximum temperature variation of C0.5-D100 increased by 2.4 times (from 18.6 to 44.7 °C) when the supply voltage increased from 30 to 60 V. In the case of C0.0-D100, the maximum temperature variation was 10.7 °C at 30 V and 23.5 °C at 60 V. When the concentration of MWCNTs of the concrete perimeter was changed from 0 to 0.5 wt% and the distance between the MWCNT heating modules was fixed at 100 mm, the maximum temperature variation increased by 1.7 times at 30 V and by 1.9 times at 60 V (Figure 11b). Therefore, the thermal performance of the slab with an MWCNT concentration of 0.5 wt% in the concrete perimeter was, at most, 1.9 times higher than that of the slab with an MWCNT concentration of 0 wt%.
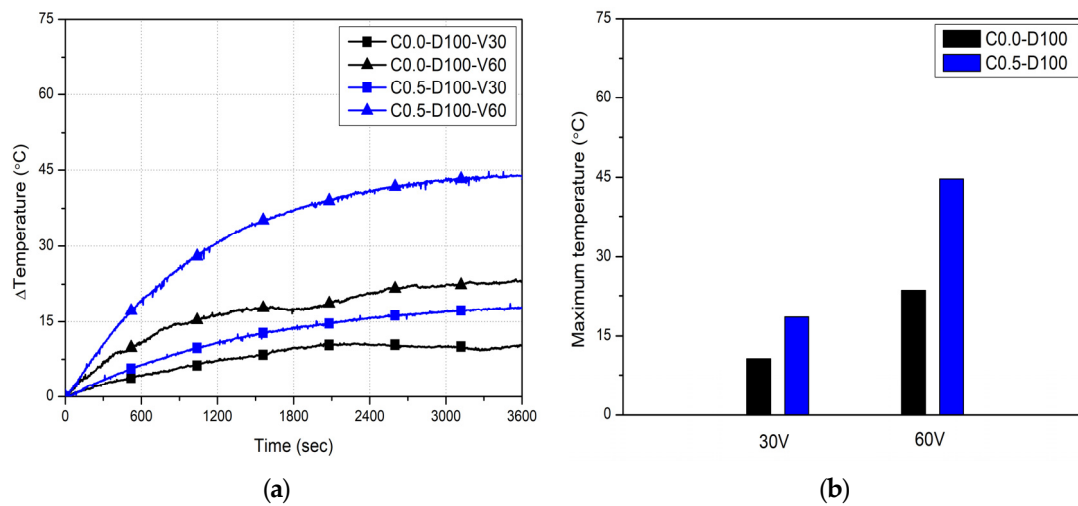
Figure 11. Temperature variation according to the concentration of MWCNTs in the full-scale test. (**a**) Temporal history. (**b**) Maximum temperature variation.

Figure 12 shows the thermal image of the slabs in the outdoor experiment. When an analysis was conducted according to the distance between the CNT heating modules, the highest temperature occurred in C0.0-D50, and the best temperature distribution was obtained in the concrete perimeter (Figure 12a). C0.0-D100 yielded a relatively lower temperature than C0.0-D50, and the temperature in the concrete perimeter was also low (Figure 12b). As shown in Figure 12c, the lowest temperature was measured in C0.0-D50, and the temperature of the concrete perimeter was also the lowest. C0.5-D100 exhibited a higher temperature than C0.0-D100, and the temperature distribution in the concrete perimeter was also excellent. In the case of the embedded concrete slab with the MWCNT heating modules, the thermal performance increased as the distance between the MWCNT heating modules decreased, and it increased following the addition of MWCNTs into the concrete perimeter.
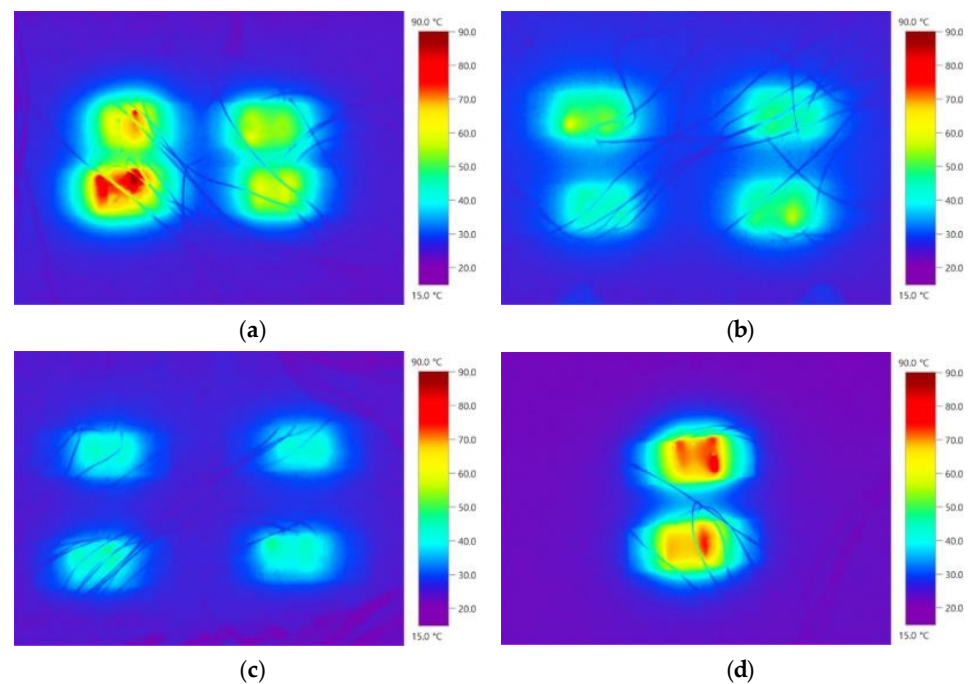
Figure 12. Thermal image of the MWCNT heating modules in the full-scale test. (**a**) C0.0-D50. (**b**) C0.0-D100. (**c**) C0.0-D150. (**d**) C0.5-D100.

4. Conclusions

In this study, a concrete slab with MWCNT heating modules inserted to solve the problem of black ice was fabricated, and thermal performance experiments were performed in indoor and outdoor environments according to the parameters (the concentration of MWCNTs in the heating module, placement interval of the MWCNT heating modules, incorporation of MWCNTs in the peripheral concrete, and the supply voltage). The indoor experiment was carried out for selection of the parameters and basic research prior to the full-scale test in an outdoor environment. Therefore, the optimal distances between MWCNT heating modules and the concentration of MWCNTs in the concrete perimeter were analyzed by conducting a laboratory test. In addition, a full-scale laboratory test was conducted on a fabricated concrete slab embedded with MWCNT heating modules in an outdoor environment. The ensuing conclusions are as follows.

(1) In the laboratory test, the thermal performance of the MWCNT heating modules increased as the concentration of MWCNTs in the concrete perimeter increased. At an MWCNT concentration of 1.0 wt%, the MWCNT heating module exhibited the most substantial maximum temperature variation, reaching 50.8 °C. Notably, despite a doubling of the amount of MWCNTs utilized at an MWCNT concentration of 1.0 wt% compared with that at 0.5 wt%, the resulting maximum difference in thermal performance was 21%. Given that the optimal thermal efficiency of the MWCNT heating module was achieved at an MWCNT concentration of 0.5 wt%, this concentration was adopted for the subsequent full-scale test.

(2) During laboratory tests, the thermal performance of the MWCNT heating module exhibited improvement as the inter-module distance decreased. The temperature variation surpassed the design threshold (17.8 °C) when the distances between the MWCNT heating modules were ≤150 mm for MWCNT concentrations of ≤0.2 wt%. Enhanced thermal performance (above the standard) was observed when the distances were ≤270 mm at a MWCNT concentration of 0.5 wt% and ≤300 mm at 1.0 wt%. It was concluded that the optimal distance between the CNT heating modules should be ≤150 mm when MWCNTs are absent from the concrete perimeter, and ≤270 mm or greater when the concentration of MWCNTs is ≥0.5 wt% during the fabrication of concrete slabs embedded with MWCNT heating modules.

(3) In the full-scale test performed in an outdoor environment, the temperature variation of the concrete slab with the MWCNT heating modules increased as the distance between these modules decreased. When the distance decreased from 150 to 50 mm, the maximum increase in temperature variation was 1.1 times. Taking into account the design temperature variation of 17.8 °C, a supply voltage exceeding 60 V was necessary when the distance was 150 mm, and excellent thermal performance was observed at a supply voltage of 60 V when the distance was ≤100 mm.

(4) For the concrete slab with the MWCNT heating modules without MWCNTs in the concrete perimeter, the maximum enhancement of the thermal performance was 2.4 times higher when the supply voltage increased from 30 to 60 V. Upon scrutinizing the trend of temperature variation among the MWCNT heating modules, it was determined that the minimum temperature criteria could be met by configuring the interval distance to values of ≤25 mm at a supply voltage of 30 V. Hence, the application of a supply voltage of 30 V to the MWCNT heating modules embedded in a concrete slab without MWCNTs in the concrete perimeter proved challenging. Nevertheless, at a supply voltage of 60 V, outstanding thermal performance was achieved when the interval distance was constrained to values of ≤125 mm. For the concrete slab with the MWCNT heating modules and without MWCNTs in the concrete perimeter, to ensure optimal performance, the supply voltage should be set to values of ≥60 V.

(5) For the concrete slab with the MWCNT heating modules in which the concentration of MWCNTs in the concrete perimeter was 0.5 wt%, the maximum temperature variation was 44.7 °C when a voltage of 60 V was applied. Accordingly, it was

1.9 times higher compared with the case in which the concentration of MWCNTs in the concrete perimeter was 0 wt%. When MWCNTs were added to the concrete perimeter, a larger temperature variation occurred owing to the improvement in the thermal conductivity of the concrete perimeter. Therefore, the addition of MWCNTs into the concrete perimeter led to higher thermal performance in the case of concrete slabs with the MWCNT heating modules.

(6) According to this research, it is expected that the long-term durability and performance test of CNT-based heating modules in the actual outdoor environment or research on alternative materials to increase the efficiency of thermal conductivity can be continued. Through these results, broader application can be extrapolated to other structures such as bridge decks and asphalt pavement repair, including the construction of heat-generating road pavements to prevent the roads icing. It can also be used as a precast with a heating module for maintenance. According to this study, the concentration and spacing of the heating modules can be adjusted according to the conditions of the construction site, and the heating performance can be adjusted by adjusting the degree of the supply voltage. Ultimately, this is expected to reduce the risk of accidents caused by the formation of black ice on road surfaces.

Author Contributions: Conceptualization, H.L. and W.C.; methodology, S.P.; investigation, H.H.; data curation, S.P.; writing—original draft preparation, H.L. and S.P.; project administration, H.L. and W.C. All authors have read and agreed to the published version of the manuscript.

Data Availability Statement: The data presented in this study are available on request from the corresponding author.

References

1. Hellstén, P.P.; Salminen, J.M.; Jørgensen, K.S.; Nystén, T.H. Use of potassium formate in road winter deicing can reduce groundwater deterioration. *Environ. Sci. Technol.* **2005**, *39*, 5095–5100. [CrossRef] [PubMed]
2. Wang, K.; Nelsen, D.E.; Nixon, W.A. Damaging effects of deicing chemicals on concrete materials. *Cem. Concr. Compos.* **2006**, *28*, 173–188. [CrossRef]
3. Kayama, M.; Quoreshi, A.M.; Kitaoka, S.; Kitahashi, Y.; Sakamoto, Y.; Maruyama, Y.; Kitao, M.; Koike, T. Effects of deicing salt on the vitality and health of two spruce species, *Picea abies* Karst, and *Picea glehnii* Masters planted along roadsides in northern Japan. *Environ. Pollut.* **2003**, *124*, 127–137. [CrossRef] [PubMed]
4. Thunqvist, E.L. Regional increase of mean chloride concentration in water due to the application of deicing salt. *Sci. Total Environ.* **2004**, *325*, 29–37. [CrossRef] [PubMed]
5. Zhao, H.; Wu, Z.; Wang, S.; Zheng, J.; Che, G. Concrete pavement deicing with carbon fiber heating wires. *Cold Reg. Sci. Technol.* **2011**, *65*, 413–420. [CrossRef]
6. Rao, R.; Fu, J.; Chan, Y.; Tuan, C.Y.; Liu, C. Steel fiber confined graphite concrete for pavement deicing. *Compos. Part B Eng.* **2018**, *155*, 187–196. [CrossRef]
7. Jiao, W.; Sha, A.; Liu, Z.; Li, W.; Zhang, L.; Jiang, S. Optimization design and prediction of the snow-melting pavement based on electrical-thermal system. *Cold Reg. Sci. Technol.* **2022**, *193*, 103406. [CrossRef]
8. Chung, D.D.L. Self-heating structural materials. *Smart Mater. Struct.* **2004**, *13*, 562. [CrossRef]
9. Wu, J.; Liu, J.; Yang, F. Three-phase composite conductive concrete for pavement deicing. *Constr. Build. Mater.* **2015**, *75*, 129–135. [CrossRef]
10. Tian, W.; Liu, Y.; Qi, B.; Wang, W. Enhanced effect of carbon nanofibers on heating efficiency of conductive cementitious composites under ohmic heating curing. *Cem. Concr. Compos.* **2021**, *117*, 103904. [CrossRef]
11. Lee, H.; Song, Y.M.; Loh, K.J.; Chung, W. Thermal response characterization and comparison of carbon nanotube-enhanced cementitious composites. *Compos. Struct.* **2018**, *202*, 1042–1050. [CrossRef]
12. Choi, K.; Min, Y.K.; Chung, W.; Lee, S.E.; Kang, S.W. Effects of dispersants and defoamers on the enhanced electrical performance by carbon nanotube networks embedded in cement-matrix composites. *Compos. Struct.* **2020**, *243*, 112193. [CrossRef]
13. Choi, K.; Kim, D.; Chung, W.; Cho, C.; Kang, S.W. Nanostructured thermoelectric composites for efficient energy harvesting in infrastructure construction applications. *Cem. Concr. Compos.* **2022**, *128*, 104452. [CrossRef]

14. Kim, G.M.; Yang, B.J.; Ryu, G.U.; Lee, H.K. The electrically conductive carbon nanotube (CNT)/cement composites for accelerated curing and thermal cracking reduction. *Compos. Struct.* **2016**, *158*, 20–29. [CrossRef]

15. Lee, H.; Park, S.; Kim, D.; Chung, W. Heating Performance of Cementitious Composites with Carbon-Based Nanomaterials. *Crystals* **2022**, *12*, 716. [CrossRef]

16. Jang, D.; Yoon, H.N.; Seo, J.; Park, S.; Kil, T.; Lee, H.K. Improved electric heating characteristics of CNT-embedded polymeric composites with an addition of silica aerogel. *Compos. Sci. Technol.* **2021**, *212*, 108866. [CrossRef]

17. Lee, H.; Yu, W.; Loh, K.J.; Chung, W. Self-heating and electrical performance of carbon nanotube-enhanced cement composites. *Constr. Build. Mater.* **2020**, *250*, 118838. [CrossRef]

18. Choi, Y.C. Cyclic heating and mechanical properties of CNT reinforced cement composite. *Compos. Struct.* **2021**, *256*, 113104. [CrossRef]

19. Kim, H.K.; Nam, I.W.; Lee, H.K. Enhanced effect of carbon nanotube on mechanical and electrical properties of cement composites by incorporation of silica fume. *Compos. Struct.* **2014**, *107*, 60–69. [CrossRef]

20. Lee, H.; Kang, D.; Kim, J.; Choi, K.; Chung, W. Void detection of cementitious grout composite using single-walled and multi-walled carbon nanotubes. *Cem. Concr. Compos.* **2019**, *95*, 237–246. [CrossRef]

21. Lee, H.; Park, S.; Park, S.; Chung, W. Enhanced detection systems of filling rates using carbon nanotube cement grout. *Nanomaterials* **2019**, *10*, 10. [CrossRef]

22. Kim, H.S.; Ban, H.; Park, W.J. Deicing concrete pavements and roads with Carbon Nanotubes (CNTs) as heating elements. *Materials* **2020**, *13*, 2504. [CrossRef]

23. Chang, C.; Ho, M.; Song, G.; Mo, Y.L.; Li, H. A feasibility study of self-heating concrete utilizing carbon nanofiber heating elements. *Smart Mater. Struct.* **2009**, *18*, 127001. [CrossRef]

24. Lee, S.H.; Kim, S.; Yoo, D.Y. Hybrid effects of steel fiber and carbon nanotube on self-sensing capability of ultra-high-performance concrete. *Constr. Build. Mater.* **2018**, *185*, 530–544. [CrossRef]

25. Hassanzadeh-Aghdam, M.K.; Mahmoodi, M.J.; Safi, M. Effect of adding carbon nanotubes on the thermal conductivity of steel fiber-reinforced concrete. *Compos. Part B Eng.* **2019**, *174*, 106972. [CrossRef]

26. Farcas, C.; Galao, O.; Navarro, R.; Zornoza, E.; Baeza, F.J.; Del Moral, B.; Pla, R.; Garcés, P. Heating and deicing function in conductive concrete and cement paste with the hybrid addition of carbon nanotubes and graphite products. *Smart Mater. Struct.* **2021**, *30*, 045010. [CrossRef]

27. Liu, Y.; Lai, Y.; Ma, D.X. Research of carbon fibre grille reinforced composites in airport pavement snowmelt. *Mater. Res. Innov.* **2015**, *19*, S10-49–S10-54. [CrossRef]

28. Lai, Y.; Liu, Y.; Ma, D. Automatically melting snow on airport cement concrete pavement with carbon fiber grille. *Cold Reg. Sci. Technol.* **2014**, *103*, 57–62. [CrossRef]

29. Ding, S.; Dong, S.; Wang, X.; Ding, S.; Han, B.; Ou, J. Self-heating ultra-high performance concrete with stainless steel wires for active deicing and snow-melting of transportation infrastructures. *Cem. Concr. Compos.* **2023**, *138*, 105005. [CrossRef]

30. Mohammed, A.G.; Ozgur, G.; Sevkat, E. Electrical resistance heating for deicing and snow melting applications: Experimental study. *Cold Reg. Sci. Technol.* **2019**, *160*, 128–138. [CrossRef]

31. Jiao, W.; Sha, A.; Liu, Z.; Jiang, W.; Hu, L.; Qin, W. Analytic investigations of snow melting efficiency and temperature field of thermal conductive asphalt concrete combined with electrical-thermal system. *J. Clean. Prod.* **2023**, *399*, 136622. [CrossRef]

32. Wan, J.; Wu, S.; Xiao, Y.; Fang, M.; Song, W.; Pan, P.; Zhang, D. Enhanced ice and snow melting efficiency of steel slag based ultra-thin friction courses with steel fiber. *J. Clean. Prod.* **2019**, *236*, 117613. [CrossRef]

33. Liu, K.; Xie, H.; Xu, P.; Wang, Z.; Bai, H.; Wang, F. The thermal and damage characteristics of an insulated-conductive composite structure for the heated bridge deck for snow-melting. *Constr. Build. Mater.* **2019**, *216*, 176–187. [CrossRef]

34. Yang, M.; Paudel, S.R.; Gao, Z.J. Snow-proof roadways using steel fiber–reinforced fly ash geopolymer mortar–concrete. *J. Mater. Civil. Eng.* **2021**, *33*, 04020444. [CrossRef]

35. Jiao, W.; Sha, A.; Liu, Z.; Li, W.; Jiang, W.; Qin, W.; Hu, Y. Study on thermal properties of steel slag asphalt concrete for snow-melting pavement. *J. Clean. Prod.* **2020**, *277*, 123574. [CrossRef]

36. Zhang, Q.; Yu, Y.; Chen, W.; Chen, T.; Zhou, Y.; Li, H. Outdoor experiment of flexible sandwiched graphite-PET sheets based self-snow-thawing pavement. *Cold Reg. Sci. Technol.* **2016**, *122*, 10–17. [CrossRef]

37. Chu, W.; Shi, X.; He, W.; Zhang, Y.; Hu, Z.; Ru, B.; Ying, S. Research on the snow melting and defogging performance of graphene heating film coupled concrete road. *Appl. Therm. Eng.* **2023**, *219*, 119689. [CrossRef]

38. Gomis, J.; Galao, O.; Gomis, V.; Zornoza, E.; Garcés, P. Self-heating and deicing conductive cement. Experimental study and modeling. *Constr. Build. Mater.* **2015**, *75*, 442–449. [CrossRef]

39. Frąc, M.; Pichór, W.; Szołdra, P.; Szudek, W. Cement composites with expanded graphite/paraffin as storage heater. *Constr. Build. Mater.* **2021**, *275*, 122126. [CrossRef]

40. Bastami, M.; Baghbadrani, M.; Aslani, F. Performance of nano-Silica modified high strength concrete at elevated temperatures. *Constr. Build. Mater.* **2014**, *68*, 402–408. [CrossRef]

41. Kočí, V.; Petříková, M.; Fořt, J.; Fiala, L.; Černý, R. Preparation of self-heating alkali-activated materials using industrial waste products. *J. Clean. Prod.* **2020**, *260*, 121116. [CrossRef]

42. Fulham-Lebrasseur, R.; Sorelli, L.; Conciatori, D. Prefabricated electrically conductive concrete (ECC) slabs with optimized electrode configuration and integrated sensor system. *Cold Reg. Sci. Technol.* **2022**, *193*, 103417. [CrossRef]

43. Galao, O.; Bañón, L.; Baeza, F.J.; Carmona, J.; Garcés, P. Highly conductive carbon fiber reinforced concrete for icing prevention and curing. *Materials* **2016**, *9*, 281. [CrossRef] [PubMed]

44. Zhang, K.; Han, B.; Yu, X. Nickel particle based electrical resistance heating cementitious composites. *Cold Reg. Sci. Technol.* **2011**, *69*, 64–69. [CrossRef]

45. Morsy, M.S.; Alsayed, S.H.; Aqel, M. Hybrid effect of carbon nanotube and nano-clay on physico-mechanical properties of cement mortar. *Constr. Build. Mater.* **2011**, *25*, 145–149. [CrossRef]

46. Sedaghatdoost, A.; Behfarnia, K. Mechanical properties of Portland cement mortar containing multi-walled carbon nanotubes at elevated temperatures. *Constr. Build. Mater.* **2018**, *176*, 482–489. [CrossRef]

47. Aodkeng, S.; Sinthupinyo, S.; Chamnankid, B.; Hanpongpun, W.; Chaipanich, A. Effect of carbon nanotubes/clay hybrid composite on mechanical properties, hydration heat and thermal analysis of cement-based materials. *Constr. Build. Mater.* **2022**, *320*, 126212. [CrossRef]

48. Lee, H.; Jeong, S.; Cho, S.; Chung, W. Enhanced bonding behavior of multi-walled carbon nanotube cement composites and reinforcing bars. *Compos. Struct.* **2020**, *243*, 112201. [CrossRef]

49. *KS L ISO 679*; Korea Agency for Technology and Standards, Methods of Testing Cements-Determination of Strength. Korea Agency for Technology and Standards: Seoul, Republic of Korea, 2006.

50. Lee, H.; Jeong, S.; Chung, W. Enhancing bond performance: Carbon fiber reinforced polymer bar interaction with multi-walled carbon nanotubes cementitious composites in chloride-exposed conditions. *Constr. Build. Mater.* **2024**, *412*, 134763. [CrossRef]

51. Barker, R.M.; Puckett, J.A. *Design of Highway Bridges Based on AASHTO LRFD Bridge Design Specifications*; John Wiley & Sons: Hoboken, NJ, USA, 1987.